

## Adiabatic and post-adiabatic approaches to extreme mass ratio inspiral

Scott A. Hughes\*

*Department of Physics and MIT Kavli Institute, MIT, Cambridge, MA 02139, USA*

*\*E-mail: sahughes@mit.edu*

Extreme mass ratio inspirals (EMRIs) show a strong separation of timescales, with the time characterizing inspiral,  $T_i$ , much longer than any time  $T_o$  characterizing orbital motions. The ratio of these timescales (which is essentially an EMRI's mass ratio) can be regarded as a parameter that controls a perturbative expansion. Here we describe the value and limitations of an “adiabatic” description of these binaries, which uses only the leading terms arising from such a two-timescale expansion. An adiabatic approach breaks down when orbits evolve through resonances, with important dynamical and observational consequences. We describe the shortfalls of an approach that only includes the adiabatic contributions to EMRI evolution, and outline what must be done to evolve these systems through resonance and to improve our ability to model EMRI systems more generally.

*Keywords:* Black holes; black hole perturbation theory; gravitational waves

### 1. Motivation: The large-mass ratio limit of the two-body problem and extreme mass ratio inspirals

Binary systems in which one body is much more massive than the other can be analyzed perturbatively. We can describe such a binary as an exact black hole solution of general relativity (corresponding to the larger member of the binary) plus a correction due to the smaller body. Because the perturbation equations are much simpler to solve than the complete equations of general relativity, this turns out to be a limit that can be modeled very accurately and precisely.

At least two major science goals drive studies of large mass ratio systems. First, these binaries represent a limit of the two-body problem that can be solved with high precision. As such, the study of these binaries provides important input to programs to solve the two-body problem of general relativity more generally, such as numerical relativity and the effective one-body approach<sup>1–3</sup>. Second, astrophysical extreme mass ratio inspirals (EMRIs) are expected to be important sources for space-based GW detectors such as eLISA<sup>4</sup> and DECIGO<sup>5</sup>.

In this article, we will focus on the role of EMRIs as sources of gravitational waves (GWs). Such binaries are created when multibody interactions scatter stellar mass compact objects onto a strong-field, relativistic orbit of the black hole in a galaxy's center. Further evolution is then driven by GW emission. If the black hole has a mass of around  $10^5 - 10^7 M_\odot$ , then these are targets for a detector like eLISA. The GWs that they generate can be heard out to  $z \sim 0.5 - 1$ ; we expect dozens to hundreds of events over a space-based detector's mission lifetime<sup>6</sup>. Measuring the GWs from these events will provide precision data on the characteristics of the large black hole, on the small body's orbit, and on the mass of the small body — in short, a precision probe of the astrophysical population of galactic center black

holes, and information about the population of stars in the centers of galaxies. It is expected that EMRI waves will even be precise enough to test the Kerr solution by mapping the multipolar structure of the dense, dark objects in galactic cores that we presume to be general relativity's black holes.

## 2. Modeling EMRIs

To achieve these science goals, we must accurately model EMRI waves. How accurate must our models be? The answer depends on the purpose to which we put the model<sup>7</sup>. The instantaneous EMRI wave amplitude will typically be about a factor of 10 smaller than detector noise. By fitting to a model template that is coherent in phase with the data for  $N$  cycles, we (roughly speaking) boost the signal-to-noise ratio (SNR) by  $N^{1/2}$ . For *detection* purposes (determining that a signal is in your data) your model should hold phase with the signal to within  $\Delta\phi \lesssim 1$  radian over the signal's duration<sup>a</sup>. The best fit is likely to have large systematic errors, but that is acceptable if our goal is just to establish that a signal is present. For *measurement* purposes (e.g., using the detected wave to determine source parameters), our model must be accurate enough that systematic errors (due to inadequate modeling) are smaller than statistic errors (due to noise). A crude rule of thumb is that the template's phase must match the signal to within  $\Delta\phi \lesssim 1/\text{SNR}$ .

Turn now to an overview of how one makes an EMRI model. We will use the action-angle approach described by Flanagan and Hinderer<sup>8</sup> to describe the motion of the small body  $m$  in the spacetime of a larger black hole of mass  $M$ :

$$\frac{dq_\alpha}{d\lambda} = \omega_\alpha(\mathbf{J}) + \varepsilon g_\alpha(q_\theta, q_r, \mathbf{J}) + O(\varepsilon^2), \quad (1)$$

$$\frac{dJ_i}{d\lambda} = \varepsilon G_i(q_\theta, q_r, \mathbf{J}) + O(\varepsilon^2). \quad (2)$$

In these equations,  $\lambda$  is a time variable that is well adapted to strong-field Kerr orbits, and  $\varepsilon = m/M$ . The angle variables

$$q_\alpha \doteq (q_t, q_r, q_\theta, q_\phi) \quad (3)$$

each describe the motion of the small body about the black hole in suitable coordinates; the action variables

$$J_i \doteq (E/m, L_z/m, Q/m^2) \quad (4)$$

correspond to integrals of the motion that are conserved along a “background” orbit (i.e., in the limit of purely geodesic motion). We will examine the forcing terms  $g_\alpha$  and  $G_i$  in more detail momentarily.

<sup>a</sup>Note that “duration” does not necessary mean the complete span of the signal in your data. One can break the data into segments, coherently integrate each segment against a template, and combine each processed segment into a single statistic.

To understand the small body's motion in this framework, let us examine Eqs. (1) and (2) more carefully. At zeroth order in  $\varepsilon$ , these equations become

$$\frac{dq_\alpha}{d\lambda} = \omega_\alpha(\mathbf{J}) , \quad \frac{dJ_i}{d\lambda} = 0 . \quad (5)$$

In other words, when the  $O(\varepsilon)$  corrections to the equations of motion are not included, the angle variables accumulate at a rate set by their associated frequency, and the integrals of the motion are constant. Equation (5) expresses the fact that the motion at zeroth order in the small body's mass is a Kerr geodesic.

When we go to the next order in  $\varepsilon$ , the forcing terms  $g_\alpha$  and  $G_i$  must be included:

$$\frac{dq_\alpha}{d\lambda} = \omega_\alpha(\mathbf{J}) + \varepsilon g_\alpha(q_\theta, q_r, \mathbf{J}) , \quad \frac{dJ_i}{d\lambda} = \varepsilon G_i(q_\theta, q_r, \mathbf{J}) . \quad (6)$$

These terms push the small body away from the geodesic, and constitute the leading self force correction to the small body's motion.

### 3. The two-timescale expansion

Further insight into EMRI evolution can be found by separating the forcing terms into their averages and oscillations about the average:

$$G_i(q_\theta, q_r, \mathbf{J}) = \langle G_i(\mathbf{J}) \rangle + \delta G_i(q_\theta, q_r, \mathbf{J}) , \quad (7)$$

where

$$\langle G_i(\mathbf{J}) \rangle = \frac{1}{(2\pi)^2} \int_0^{2\pi} dq_\theta \int_0^{2\pi} dq_r G_i(q_\theta, q_r, \mathbf{J}) , \quad (8)$$

$$\delta G_i(q_\theta, q_r, \mathbf{J}) = G_i(q_\theta, q_r, \mathbf{J}) - \langle G_i(\mathbf{J}) \rangle . \quad (9)$$

We apply a similar split to  $g_\alpha(q_\theta, q_r, \mathbf{J})$ . Rewrite the equations of motion once more:

$$\frac{dq_\alpha}{d\lambda} = \omega_\alpha(\mathbf{J}) + \varepsilon \langle g_\alpha(\mathbf{J}) \rangle + \varepsilon \delta g_\alpha(q_\theta, q_r, \mathbf{J}) , \quad (10)$$

$$\frac{dJ_i}{d\lambda} = \varepsilon \langle G_i(\mathbf{J}) \rangle + \varepsilon \delta G_i(q_\theta, q_r, \mathbf{J}) . \quad (11)$$

The averaged forcing term  $\langle G_i(\mathbf{J}) \rangle$  describes the leading evolution of the small body's integrals of motion; its components describe the dissipative evolution of  $E$ ,  $L_z$ , and  $Q$ . This term drives the secular evolution of the system's orbital parameters on an inspiral time scale  $T_i \sim M/\varepsilon = M^2/m$ . The averaged forcing term  $\langle g_\alpha(\mathbf{J}) \rangle$  is equivalent to a shift of the frequencies:

$$\omega_\alpha(\mathbf{J}) \longrightarrow \omega_\alpha(\mathbf{J}) + \varepsilon \langle g_\alpha(\mathbf{J}) \rangle . \quad (12)$$

This shift is the leading conservative contribution of the small body's self force. These forcing terms are nearly constant, varying on the long timescale  $T_i \sim M^2/m$  that characterizes the rate of change of the integrals of motion  $\mathbf{J}$ . By contrast, the forcing terms  $\delta G_i(q_\theta, q_r, \mathbf{J})$  and  $\delta g_\alpha(q_\theta, q_r, \mathbf{J})$  vary rapidly on a timescale  $T_o \sim M$  that characterizes the small body's orbital motion. Their impact is (usually) much less important than the impact of the averaged terms  $\langle G_i(\mathbf{J}) \rangle$  and  $\langle g_\alpha(\mathbf{J}) \rangle$ .

As discussed above, the most important detail we need to understand to characterize models for GW measurements is the phase<sup>b</sup> accumulated over some interval:

$$\Phi(t_1, t_2) = \int_{t_1}^{t_2} \omega(t) dt = \Phi_{\text{diss}-1} + \Phi_{\text{cons}-1} + \Phi_{\text{diss}-2} + \Phi_{\text{cons}-2} + \dots \quad (13)$$

The contributions to this phase have the following scalings with masses, and arise from the following pieces of source physics:

- $\Phi_{\text{diss}-1} = O(T_i/T_o) = O(M/m)$ : The slowing evolving geodesic frequency  $\omega = 1/T_o \sim 1/M$  integrated over the inspiral time  $T_i \sim M^2/m$ .
- $\Phi_{\text{cons}-1} = O(\epsilon T_i/T_o) = O(1)$ : The conservative correction to the frequency  $\delta\omega \sim \epsilon\omega$  integrated over the inspiral time  $T_i$ .
- $\Phi_{\text{diss}-2} = O(\epsilon T_i/T_o) = O(1)$ : The slowly evolving geodesic frequency  $\omega$  integrated against the oscillatory correction to the inspiral time  $\delta T_i \sim \epsilon T_i$ .
- $\Phi_{\text{cons}-2} = O(\epsilon^2 T_i/T_o) = O(m/M)$ : The conservative correction to the frequency  $\delta\omega \sim \epsilon\omega$  integrated against the oscillatory correction to the inspiral time  $\delta T_i \sim \epsilon T_i$ .

These schematic countings suggest that we must include the leading adiabatic conservative piece and perhaps the first oscillatory dissipative piece in order to have effective *detection* templates. We certainly will need to go farther for measurement purposes, or else just accept that a certain level of systematic error may be very difficult to remove from EMRI waveform models.

#### 4. Adiabaticity and its limitations: Resonant orbits

The fact that the oscillatory contributions to the EMRI model are subleading suggests that a useful approximation may be to ignore them at first pass. Doing so gives us the *adiabatic approximation* to EMRI evolution:

$$\frac{dq_\alpha}{d\lambda} = \omega_\alpha(\mathbf{J}) + \epsilon \langle g_\alpha(\mathbf{J}) \rangle, \quad \frac{dJ_i}{d\lambda} = \epsilon \langle G_i(\mathbf{J}) \rangle. \quad (14)$$

For *most* black hole orbits, this approximation works well. This is because the small body's motion typically is ergodic: after a small number of orbits (requiring far less than the inspiral time), the small body has come close to every point it is allowed to pass through. Its motion thus averages the forcing terms in the equations of motion more or less automatically. This is illustrated in the left-hand panel of Fig. 1 (adapted from Fig. 1 of Ref. 9), which shows the path in  $(r, \theta)$  traced out by an orbit. Roughly nine radial orbits are shown here. Given enough time, this trace would fill the entire  $(r, \theta)$  plane over the domain  $2M \lesssim r \lesssim 12M$ ,  $70^\circ \leq \theta \leq 110^\circ$ .

However, there exist orbits for which this averaging does not occur. If the small body's  $\theta$  and  $r$  frequencies are in a low-order resonance, then the motion is not

<sup>b</sup>Bear in mind that the following equation is meant to be schematic. The frequency  $\omega(t)$  which appears under this integral is in fact a harmonic of the various frequencies which characterize Kerr black hole orbits, and as such has more contributions than are indicated in this sketch.

ergodic, but instead traces out a Lissajous figure in the  $(r, \theta)$  plane. An example is shown in the right-hand panel of Fig. 1. Because these orbits do not come close to all allowed points in the accessible physical space, they do not effectively average the forcing functions  $g_\alpha(q_\theta, q_r, \mathbf{J})$  and  $G_i(q_\theta, q_r, \mathbf{J})$ . Indeed, different initial conditions trace out different Lissajous figures. This means that the detailed manner in which averaging fails depends on an orbit's phase as it enters resonance.

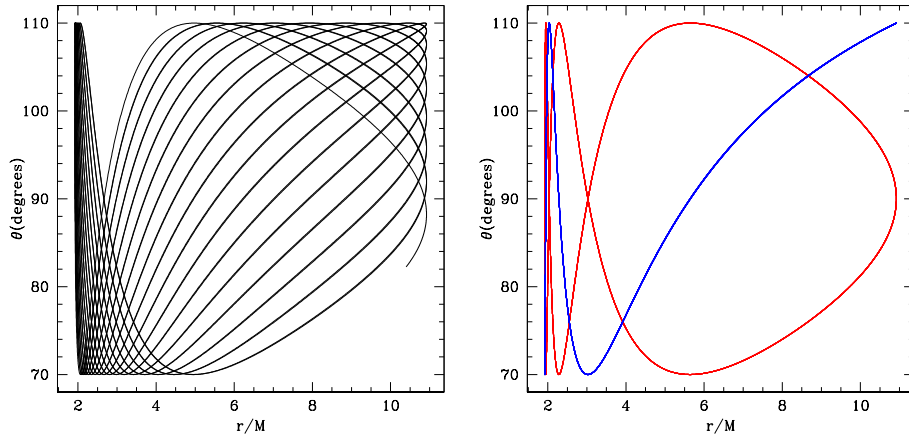


Fig. 1. Three example Kerr black hole orbits. All oscillate between  $2M \lesssim r \lesssim 12M$  and  $70^\circ \leq \theta \leq 110^\circ$ ; roughly 9 radial cycles are shown for each case. The left-hand panel shows these orbits for a black hole with spin parameter  $a = 0.95M$ . This motion is ergodic — given enough time, the orbit would come arbitrarily close to every accessible point in  $(r, \theta)$ . The right-hand panel shows two orbits for spin  $a = 0.9M$ . The  $\theta$  and  $r$  motions of these orbits are in a 3:1 resonance: the orbit oscillates three times in  $\theta$  over each radial cycle. No matter how long we wait, the motion will be confined to the Lissajous figures shown here. The particular points the orbit passes through depend on the system's phase as it enters resonance. Two examples are shown here.

To make this more quantitative, examine the Fourier expansion of  $G_i$ :

$$G_i(q_\theta, q_r, \mathbf{J}) = \sum_{kn} G_{i;kn}(\mathbf{J}) e^{i(kq_\theta + nq_r)}. \quad (15)$$

For a non-resonant orbit, only one term on the right-hand survives averaging: using Eq. (8), we have

$$\langle G_i(\mathbf{J}) \rangle_{\text{non-res}} = G_{i;00}(\mathbf{J}). \quad (16)$$

since  $\langle e^{i(kq_\theta + nq_r)} \rangle = 0$  except for  $k = n = 0$ .

This is not the case for resonant orbits. When  $\Omega_\theta/\Omega_r$  are in a ratio of small integers, then  $q_\theta/q_r$  are also in a ratio of small integers. We now find that many terms on the right-hand side of Eq. (15) survive the average:

$$\langle G_i(\mathbf{J}) \rangle_{\text{res}} = G_{i;00}(\mathbf{J}) + \sum_{(k,n)} G_{i;kn}. \quad (17)$$

The final sum is over all pairs  $(k, n)$  that satisfy  $kq_\theta + nq_r = 0$ .

Averaging, and thus the adiabatic approximation, fails as we enter a resonance. The oscillatory terms in the equations of motion combine in phase on a resonance, “kicking” the system until it evolves away from the resonance. The adiabatic evolution does well at describing the system’s evolution before and after the resonance, but does a poor job at modeling in the system very near the resonance. Taking resonances into account, we find that the system’s phase evolution must be modified:

$$\begin{aligned}\Phi(t_1, t_2) &= \int_{t_1}^{t_2} \omega(t) dt \\ &= \Phi_{\text{diss}-1} + \Phi_{\text{RES}} + \Phi_{\text{cons}-1} + \Phi_{\text{diss}-2} + \Phi_{\text{cons}-2} + \dots\end{aligned}\quad (18)$$

This form is identical to that given earlier, but there is now a new term:  $\Phi_{\text{RES}} = O(\epsilon^{1/2} T_i/T_o) = O([M/m]^{1/2})$ . *This term dominates over all but the leading dissipative contributions to the system’s phase evolution.* Detailed analysis<sup>10,11</sup> indeed shows that  $\Phi_{\text{RES}}$  contributes dozens to hundreds of radians to the system’s phase evolution, substantially more than all terms except the leading one.

One might imagine that, since resonant orbits are a set of measure zero in the complete set of Kerr black hole orbits, these cases are curiosities that are unlikely to play much role in astrophysics. That is not the case. Consider a set of astrophysical inspirals with parameters such that they are likely to be important sources for low-frequency GW detector. We have shown<sup>11</sup> that *every* inspiral will pass through at least one dynamically significant low-order resonance as it spirals through the detector’s sensitive band. Many of these inspirals will pass through two significant resonances; some will pass through three.

## 5. Summary and outlook

Although useful for producing a somewhat accurate picture of extreme mass ratio binaries, the adiabatic approach to inspiral is ultimately inadequate for modeling these sources, even for the less stringent task of developing detection templates. We must go beyond this picture and develop post-adiabatic EMRI models in order to more completely model these sources.

Of particular importance is understanding the magnitude of the “kick” that is imparted to an EMRI’s evolution by each resonance passage. Properly doing this requires that we self consistently integrate the equations of motion, including the oscillatory part of the self interaction. Past work<sup>9–11</sup> has given us some idea how much kick we can expect and the number of cycles over which the kick operates, but it remains important to develop a fully self consistent inspiral and waveform model to assess the reliability of these estimates.

Even with good modeling, it is likely that the impact of resonances will substantially complicate our ability to measure EMRI GWs. The detailed evolution of an EMRI on resonance depends on the value of two orbital phases as we enter resonance. For non-resonant orbits, these phases are ignorable. Resonances thus in-

crease the dimensionality of the EMRI waveform manifold, and potentially greatly expand the number of parameters that will be needed for measurement templates.

For detection purposes at least, it may be adequate to break the data into segments. A simple, adiabatic model suffices to model the system's phase until we are within a few dozen or hundred radians of the resonance; a different simple, adiabatic model suffices to model the phase once we are a few dozen or hundred radians past resonance. Each EMRI is thus broken into pre- and post-resonance segments. Similar techniques are used in radio astronomy to model glitching pulsars, when a pulsar's spin frequency suddenly changes following a change in a neutron star's moment of inertia due to a rearrangement of its internal fluid distribution (see, e.g., Fig. 1 of Ref. 12 for an example and discussion). This segmented approach is likely to work well on EMRI events whose fully coherent signal-to-noise ratios are several tens or larger.

Much work remains to be done on this challenging problem.

### Acknowledgments

Research in our group is supported by National Science Grant PHY-1403261. The work discussed here has been done in collaboration with Éanna Flanagan and Uchupol Ruangsri, and has benefitted greatly from discussions with Tanja Hinderer, Eric Poisson, and Niels Warburton.

### References

1. L. Lehner and F. Pretorius, *Ann. Rev. Astron. Astrophys.* **52**, 661 (2014).
2. U. Sperhake, *Class. Quantum Grav.* **32**, 124011 (2015).
3. T. Damour, in Proceedings of the conference “Relativity and Gravitational — 100 years after Einstein in Prague,” arXiv:1212.3159.
4. The eLISA Consortium (P. Amaro Seoane et al.), *The Gravitational Universe*, arXiv:1305.5720.
5. K. Yagi, *Int. J. Mod. Phys. D* **22**, 1341013 (2013).
6. P. Amaro-Seoane, J. R. Gair, A. Pound, S. A. Hughes, and C. F. Sopuerta, *J. of Phys.: Conf. Ser.* **610**, 012002 (2015).
7. L. Lindblom, B. J. Owen, and D. A. Brown, *Phys. Rev. D* **78**, 124020 (2008).
8. T. Hinderer and E. E. Flanagan, *Phys. Rev. D* **78** 064028 (2008).
9. E. E. Flanagan, S. A. Hughes, and U. Ruangsri, *Phys. Rev. D* **89**, 084028 (2014).
10. E. E. Flanagan and T. Hinderer, *Phys. Rev. Lett.* **109**, 071102 (2012).
11. U. Ruangsri and S. A. Hughes, *Phys. Rev. D* **89**, 084036 (2014).
12. B. Link, R. I. Epstein, and K. A. van Riper, *Nature* **359**, 616 (1992).